

Chapter 2

Mathematical Model of the Safety Factor and Control Problem Formulation

We are interested in controlling the safety factor profile in a tokamak plasma. As the safety factor depends on the ratio of the normalized radius to the poloidal magnetic flux gradient, controlling the gradient of the magnetic flux allows controlling the safety factor profile. In this chapter we present the reference dynamical model [1] for the poloidal magnetic flux profile and its gradient (equivalent to the effective poloidal field magnitude, as defined in [2]), used throughout the following chapters, as well as the control problem formulation. Some of the main difficulties encountered when dealing with this problem are also highlighted.

2.1 Inhomogeneous Transport of the Poloidal Magnetic Flux

The poloidal magnetic flux, denoted $\psi(R, Z)$, is defined as the flux per radian of the magnetic field $B(R, Z)$ through a disc centered on the toroidal axis at height Z , having a radius R , see Fig. 2.1. A simplified one-dimensional model for this poloidal magnetic flux profile is considered. Its dynamics is given by the following equation [3]:

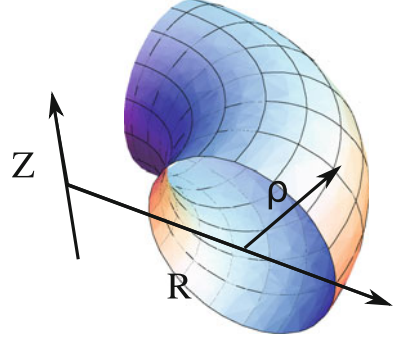
$$\frac{\partial \psi}{\partial t} = \frac{\eta_{\parallel} C_2}{\mu_0 C_3} \frac{\partial^2 \psi}{\partial \rho^2} + \frac{\eta_{\parallel} \rho}{\mu_0 C_3^2} \frac{\partial}{\partial \rho} \left(\frac{C_2 C_3}{\rho} \right) \frac{\partial \psi}{\partial \rho} + \frac{\eta_{\parallel} \frac{\partial \mathcal{V}}{\partial \rho} B_{\phi_0}}{F C_3} j_{ni} \quad (2.1)$$

with the geometry defined by:

$$\rho \doteq \sqrt{\frac{\phi}{\pi B_{\phi_0}}}, \quad C_2(\rho) \doteq \frac{\partial \mathcal{V}}{\partial \rho} \left\langle \frac{\|\rho\|^2}{R^2} \right\rangle, \quad C_3(\rho) \doteq \frac{\partial \mathcal{V}}{\partial \rho} \left\langle \frac{1}{R^2} \right\rangle$$

where $\langle \cdot \rangle$ represents the average over a flux surface, indexed by the equivalent radius ρ . The remaining coefficients are: ϕ , the toroidal magnetic flux; B_{ϕ_0} , the value of the toroidal magnetic flux at the plasma center; η_{\parallel} , the parallel resistivity of the plasma; and μ_0 , the permeability of free space. j_{ni} is a source term representing the

Fig. 2.1 Coordinate system (R, Z) used in this chapter



total effective current produced by non-inductive current sources. F is the diamagnetic function and $\frac{\partial \mathcal{V}}{\partial \rho}$ is the spatial derivative of the plasma volume enclosed by the magnetic surface indexed by ρ . A summary of these variables can be found in Appendix B.

With the following simplifying assumptions:

- $\rho \ll R_0$ (usually referred to as the cylindrical approximation, where R_0 is the major radius of the plasma);
- the diamagnetic effect caused by poloidal currents can be neglected, the coefficients C_2 , C_3 and F simplify to:

$$F \approx R_0 B_{\phi_0}, \quad C_2(\rho) = C_3(\rho) = 4\pi^2 \frac{\rho}{R_0}$$

and the spatial derivative of the enclosed plasma volume becomes:

$$\frac{\partial \mathcal{V}}{\partial \rho} = 4\pi^2 \rho R_0$$

Introducing the normalized variable $r \doteq \rho/a$, a being the minor radius of the last closed magnetic surface, we obtain the simplified model [1, 4]:

$$\frac{\partial \psi}{\partial t}(r, t) = \frac{\eta_{\parallel}(r, t)}{\mu_0 a^2} \left(\frac{\partial^2 \psi}{\partial r^2} + \frac{1}{r} \frac{\partial \psi}{\partial r} \right) + \eta_{\parallel}(r, t) R_0 j_{ni}(r, t) \quad (2.2)$$

with the boundary condition at the plasma center:

$$\frac{\partial \psi}{\partial r}(0, t) = 0 \quad (2.3)$$

one of the two boundary conditions at the plasma edge:

$$\frac{\partial \psi}{\partial r}(1, t) = -\frac{R_0 \mu_0 I_p(t)}{2\pi} \quad \text{or} \quad \frac{\partial \psi}{\partial t}(1, t) = V_{loop}(t) \quad (2.4)$$

(where I_p is the total plasma current and V_{loop} is the toroidal loop voltage) and with the initial condition:

$$\psi(r, t_0) = \psi_0(r)$$

Remark 2.1 The validity of this model (derived for Tore Supra) can be extended to other tokamaks by changing the definition of the values C_2 , C_3 , F and $\frac{\partial \mathcal{V}}{\partial \rho}$.

2.2 Periferal Components Influencing the Poloidal Magnetic Flux

The dynamics (2.2) depend on the plasma resistivity (diffusion coefficient), the inductive current generated by the poloidal coils (boundary control input) and the non-inductive currents (distributed control input and nonlinearity), which can be described as follows.

2.2.1 Resistivity and Temperature Influence

The diffusion term in the magnetic flux dynamics is provided by the plasma resistivity $\eta_{||}$, which introduces a coupling with the temperature (main influence) and density profiles. This parameter is obtained from the neoclassical conductivity proposed in [5] (approximate analytic approach) using the electron thermal velocity and Braginskii time, computed from the temperature and density profiles as in [6].

The temperature dynamics are typically determined by a resistive-diffusion equation [2], where the diffusion coefficient depends nonlinearly on the safety factor profile [7]. A quasi-1D model was proposed in [8] to model the normalized temperature profiles as scaling laws determined by the global (0-D) plasma parameters and to constrain the temperature dynamics by the global energy conservation. This grey-box model was shown to provide a sufficient accuracy for the magnetic flux prediction in [1].

The resistive-diffusion time is much faster (more than 10 times) than the current density diffusion time, which motivated lumped control approaches based on the separation of the timescales and using a linear time-invariant model [9, 10]. In our case, we consider that $\eta_{||}$ varies in time and space, to avoid the strong dependency on the operating point, but we do not address specifically the problem of a coupling with the temperature dynamics (thus considering only the linear time-varying contribution of the resistivity).

As an example, the resistivity calculated with measured temperature profiles is depicted in Fig. 2.2. This plasma shot is characterized by power modulations of the

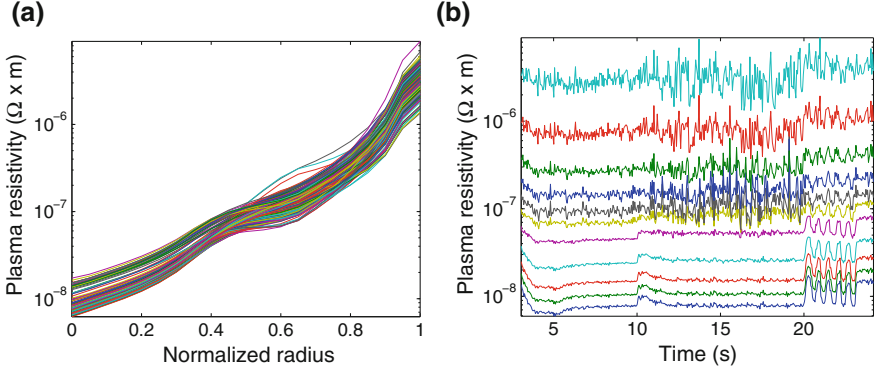


Fig. 2.2 **a** Spatial distribution for different time instants. **b** Time evolution at different locations. Plasma resistivity profiles computed for Tore Supra shot 35952 (modulations on the LH and ICRH antennas)

lower hybrid (LH) and ion cyclotron radio heating (ICRH) antennas. Note the difference of three orders of magnitude between the plasma center and its edge on Fig. 2.2a, and the modulated and noisy time-evolution on Fig. 2.2b. The crevells observed after 20 s result from LH modulations (step inputs) at relatively low power and illustrate an input-to-state coupling effect, as LH is our main input on the magnetic flux.

2.2.2 Inductive Current Sources

The magnetic flux at the boundary $\frac{\partial}{\partial t} \psi(1, t)$ is set by the poloidal coils surrounding the plasma and the central solenoid, and constitutes the inductive current input. This can be described by the classical transformer model where the coils generate the primary circuit while the plasma is the secondary, modelled as a single filament. The dynamics of the coils current $I_c(t)$ and of the plasma current $I_p(t)$ are coupled as [11]:

$$\begin{bmatrix} L_c & M \\ M & L_p \end{bmatrix} \frac{d}{dt} \begin{bmatrix} I_c \\ I_p \end{bmatrix} = - \begin{bmatrix} R_c & 0 \\ 0 & R_p \end{bmatrix} \begin{bmatrix} I_c \\ I_p \end{bmatrix} + \begin{bmatrix} V_c \\ R_p I_{NI} \end{bmatrix}$$

where R_c and L_c are the coils resistance and internal inductance, R_p and L_p are the plasma resistance and inductance, M is the matrix of mutual inductances, V_c is the input voltage applied to the coils and I_{NI} is the current generated by the non-inductive sources. Note that the values of R_c and L_c are given from the coil properties while M is obtained from an equilibrium code (i.e. CEDRES++ [12]). Considering the effects of the plasma current and inductance variations, the loop voltage V_{loop} is obtained from [13] with:

$$V_{loop}(t) = -\frac{1}{I_p} \frac{d}{dt} \left[\frac{L_p I_p^2}{2} \right] + M \frac{dI_c}{dt}$$

In practice, a local control law is set on the poloidal coils to adjust the value of V_c according to a desired value of V_{loop} , which can be measured with a Rogowski coil. If the reference is set on the plasma current I_p instead, then V_c is such that the coils provide the current necessary for completing the non inductive sources to obtain I_p .

2.2.3 Non-inductive Current: Sources and Nonlinearity

The non-inductive current j_{ni} in the magnetic flux dynamics (2.2) is composed of two types of sources: the controlled inputs and the bootstrap effect.

The controlled inputs are the current drive (CD) effects associated with neutral beam injection (NBI), traveling waves in the lower hybrid (LH) frequency range (0.8–8 GHz, the most effective scheme) and electron cyclotron (EC) waves. The precise physical modeling of the CD effects necessitates a complex analysis of the coupling between waves and particles, which cannot be used for real-time control purposes. We consider instead some semi-empirical models for the Lower Hybrid Current Drive (LHCD) and Electron Cyclotron Current Drive (ECCD) antennas (NBI is not explicitly included in our control schemes but the general strategy would remain the same), where the current deposit shape is constrained to fit a gaussian bell [1]. The gaussian shape is identified from experimental data (LHCD) or obtained from model simplifications (ECCD), while the amplitude of the deposit comes from CD efficiency computations involving the density, temperature and total current of the plasma.

For example the shape of LHCD deposit can be adequately approximated by a gaussian curve with parameters μ , σ and A_{lh} (which depend on the engineering parameters P_{lh} and $N_{||}$ and on the operating point) as:

$$j_{lh}(r, t) = A_{lh}(t) e^{-(r-\mu(t))^2/(2\sigma^2(t))}, \forall(r, t) \in [0, 1] \times [0, T] \quad (2.5)$$

Scaling laws for the shape parameters can be built based on suprathermal electron emission, measured via hard X-ray measurements, see for instance [14] and [15]. The total current driven by the LH antenna is then calculated using scaling laws such as those presented in [16]. It should be noted that the methods presented in this book can easily be extended to other current deposit shapes (either for use in other tokamaks or to change the non-inductive current drives used).

While the impact of I_p on the deposit amplitude would induce a nonlinearity (product between the state and the control input), we neglect this effect by considering an extra loop on the radio-frequency antennas that sets the engineering inputs according to a desired profile. Such strategy is motivated by the fact that the antennas react much faster than the plasma and can thus generate a desired profile almost instantly.

The second non-inductive source of current is due to the bootstrap effect, induced by particles trapped in a banana orbit. Expressing the physical model derived by [17] in cylindrical coordinates and in terms of the magnetic flux, the bootstrap current is obtained as:

$$j_{bs}(r, t) = \frac{p_e R_0}{\partial \psi / \partial r} \left\{ A_1 \left[\frac{1}{p_e} \frac{\partial p_e}{\partial r} + \frac{p_i}{p_e} \left(\frac{1}{p_i} \frac{\partial p_i}{\partial r} - \alpha_i \frac{1}{T_i} \frac{\partial T_i}{\partial r} \right) \right] - A_2 \frac{1}{T_e} \frac{\partial T_e}{\partial r} \right\}$$

where $p_{e/i}$ is the electron and ion pressure, $T_{e/i}$ is the electron and ion temperature, α_i depends on the ratio of trapped to circulating particles x_t and $A_{1/2}(r, t)$ depend on x_t and on the effective value of the plasma charge. Maximizing the bootstrap effect, as a “free” source of non-inductive current, is one of the prime objectives for large tokamaks such as ITER, which motivated the bootstrap current maximization strategy proposed in [18]. As the control approaches discussed in this book are focused on linear time-varying strategies (on the lumped and PDE models), we will consider small deviations from an equilibrium bootstrap distribution (given by the reference magnetic flux distribution) and ensure the robustness with respect to these deviations rather than addressing the nonlinearity directly.

To summarize, j_{ni} is considered as the sum of three components:

$$j_{ni} = j_{lh} + j_{eccd} + j_{bs}$$

2.3 Control Problem Formulation

Based on the previous description of the system dynamics and periferal components obtained from a physical analysis of the tokamak plasma, this section discusses the appropriate change of variables to formulate the control problem. We also describe the control objectives and challenges for an efficient regulation of the safety-factor profile, which will be answered in the following chapters.

2.3.1 Equilibrium and Regulated Variation

We define $\eta \doteq \eta_{\parallel} / \mu_0 a^2$ and $j \doteq \mu_0 a^2 R_0 j_{ni}$ to simplify the notations. An equilibrium $\bar{\psi}$, if it exists, is defined as a stationary solution of:

$$0 = \left[\frac{\eta}{r} [r \bar{\psi}_r]_r \right]_r + [\eta \bar{j}]_r, \forall r \in (0, 1) \quad (2.6)$$

with the boundary conditions:

$$\begin{aligned}\bar{\psi}_r(0) &= 0 \\ \bar{\psi}_r(1) &= -\frac{R_0\mu_0\bar{I}_p}{2\pi}\end{aligned}\tag{2.7}$$

for a given couple (\bar{j}, \bar{I}_p) , where, to simplify the notation, for any function ξ depending on the independent variables r and t , ξ_r and ξ_t are used to denote $\frac{\partial \xi}{\partial r}$ and $\frac{\partial \xi}{\partial t}$, respectively.

Remark 2.2 When seeking an equilibrium by solving (2.6)–(2.7) two cases have to be considered:

- (i) there is no drift in $\bar{\psi}$ (equivalent to $V_{loop} = 0$ at all times using the alternative boundary condition $\psi_t(1, t) = V_{loop}(t)$ in (2.4)) and therefore the solution of (2.6)–(2.7) verifies:

$$\frac{\eta}{r} [r\bar{\psi}_r]_r + \eta\bar{j} = 0\tag{2.8}$$

In this case, $\bar{\psi}$ (and its spatial derivative) is independent on the value of η and therefore the stationary solution exists (i.e. there is an equilibrium of the time-varying system) regardless of the variations in η . This is the case we directly address in this book.

- (ii) there is a radially constant drift in $\bar{\psi}$ (equivalent to $V_{loop} \neq 0$ for some times when using the alternative boundary condition) and therefore the solution of (2.6)–(2.7) verifies, for some $c(t)$:

$$\frac{\eta(r, t)}{r} [r\bar{\psi}_r(r, t)]_r + \eta(r, t)\bar{j}(r) = c(t)\tag{2.9}$$

In this case, $\bar{\psi}_r$ does not correspond to an equilibrium since it will be a function of time and space (in particular, it will be a function of $\eta(r, t)$ and $c(t)$), we will call the corresponding $\bar{\psi}(r, t)$ a pseudo-equilibrium of the system. It can be shown to verify:

$$\bar{\psi}_r(r, t) = \frac{1}{r} \int_0^r \left(\frac{\rho}{\eta(\rho, t)} c(t) - \rho\bar{j}(\rho) \right) d\rho\tag{2.10}$$

with time-derivative:

$$\bar{\psi}_{rt}(r, t) = \frac{1}{r} \int_0^r \left(\frac{\rho}{\eta(\rho, t)} \dot{c}(t) - \frac{\rho\dot{\eta}(\rho, t)}{\eta^2(\rho, t)} c(t) \right) d\rho\tag{2.11}$$

This case is not extensively addressed in this book but the results presented in Chaps. 4 and 5 will not be severely affected as long as $\dot{c}(t)$ and $\dot{\eta}(r, t)$ are bounded in a suitable way. Since a pseudo-equilibrium will exist at each time,

the robustness result presented in Theorem 4.2 can be applied, rewriting the evolution of the system around this pseudo-equilibrium (instead of an actual equilibrium) and considering $w = -\bar{\psi}_{rt}(r, t)$ (the time-varying nature of the pseudo-equilibrium acts as a state-disturbance for the system).

Around the equilibrium (assumed to exist as per the previous remark) and neglecting the nonlinear dependence of the bootstrap current on the state, the dynamics of the system is given by:

$$\tilde{\psi}_t = \frac{\eta}{r} \left[r \tilde{\psi}_r \right]_r + \eta \tilde{j}, \quad \forall (r, t) \in (0, 1) \times (0, T) \quad (2.12)$$

with boundary conditions:

$$\begin{aligned} \tilde{\psi}_r(0, t) &= 0 \\ \tilde{\psi}_r(1, t) &= -\frac{R_0 \mu_0 \tilde{I}_p(t)}{2\pi} \end{aligned} \quad (2.13)$$

and initial condition:

$$\tilde{\psi}(r, 0) = \tilde{\psi}_0(r) \quad (2.14)$$

where the dependence of $\tilde{\psi} \doteq \psi - \bar{\psi}$, $\tilde{j} \doteq j - \bar{j}$ and η on (r, t) is implicit; $\tilde{I}_p \doteq I_p - \bar{I}_p$ and $0 < T \leq +\infty$ is the time horizon.

As the safety factor profile depends on the magnetic flux gradient, our focus is on the evolution of $z \doteq \partial \tilde{\psi} / \partial r$ (equivalent to deviations of the effective poloidal field magnitude around an equilibrium), with input $u \doteq \tilde{j}$, defined as:

$$z_t(r, t) = \left[\frac{\eta(r, t)}{r} [r z(r, t)]_r \right]_r + [\eta(r, t) u(r, t)]_r, \quad \forall (r, t) \in (0, 1) \times (0, T) \quad (2.15)$$

with Dirichlet boundary conditions:

$$\begin{aligned} z(0, t) &= 0 \\ z(1, t) &= -\frac{R_0 \mu_0 \tilde{I}_p(t)}{2\pi} \end{aligned} \quad (2.16)$$

and initial condition:

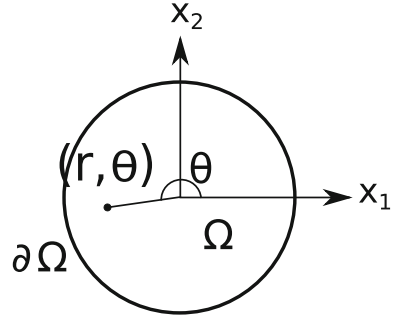
$$z(r, 0) = z_0(r) \quad (2.17)$$

where $z_0 \doteq \left[\tilde{\psi}_0 \right]_r$.

Following [19], the following properties are assumed to hold in (2.15):

- **P₁**: $K \geq \eta(r, t) \geq k > 0$ for all $(r, t) \in [0, 1] \times [0, T)$ and some positive constants k and K .

Fig. 2.3 Cartesian coordinates (x_1, x_2) , and polar coordinates (r, θ) used in this book



- **P₂**: The two-dimensional Cartesian representations of η and u are in $C^{1+\alpha_c, \alpha_c/2}(\overline{\Omega} \times [0, T])$, $0 < \alpha_c < 1$, where $\Omega \doteq \{(x_1, x_2) \in \mathbb{R}^2 \mid x_1^2 + x_2^2 < 1\}$ as shown in Fig. 2.3.
- **P₃**: \tilde{I}_p is in $C^{(1+\alpha_c)/2}([0, T])$.

For completeness purposes, the existence and uniqueness of sufficiently regular solutions (as needed for the Lyapunov analysis and feedback design purposes in the next chapters) of the evolution equation is stated, assuming that the properties P_1 – P_3 are verified.

Theorem 2.1 *If Properties P_1 – P_3 hold then, for every $z_0 : [0, 1] \rightarrow \mathbb{R}$ in $C^{2+\alpha_c}([0, 1])$ ($0 < \alpha_c < 1$) such that $z_0(0) = 0$ and $z_0(1) = -R_0\mu_0\tilde{I}_p(0)/2\pi$, the evolution equations (2.15)–(2.17) have a unique solution $z \in C^{1+\alpha_c, 1+\alpha_c/2}([0, 1] \times [0, T]) \cap C^{2+\alpha_c, 1+\alpha_c/2}([0, 1] \times [0, T])$.*

The proof of this result is given in [19] and mainly follows from [20].

2.3.2 Interest of Choosing ψ as the Regulated Variable

A natural question that may arise at this point is why studying the evolution of the poloidal magnetic flux profile instead of studying directly the safety factor profile. Considering that the safety factor profile is related to the magnetic flux profile as:

$$q(r, t) = -\frac{B_{\phi_0} a^2 r}{\psi_r(r, t)} \quad (2.18)$$

the evolution of the safety factor profile is then given by:

¹ Here $C^{\alpha_c, \beta_c}(\overline{\Omega} \times [0, T])$ denotes the space of functions which are α_c -Hölder continuous in $\overline{\Omega}$, β_c -Hölder continuous in $[0, T]$. P_2 can be strengthened by assuming that η and u are in $C^{2,1}(\overline{\Omega} \times [0, T])$ which is the case for the physical application.

$$q_t(r, t) = \frac{B_{\phi_0} a^2 r}{\psi_r^2(r, t)} \psi_{rt}(r, t) = \frac{q^2(r, t)}{B_{\phi_0} a^2 r} \psi_{rt}(r, t)$$

and, from (2.2):

$$q_t(r, t) = -\frac{q^2(r, t)}{r} \left[\frac{\eta(r, t)}{r} \left[\frac{r^2}{q(r, t)} \right]_r \right]_r + \frac{q^2(r, t)}{B_{\phi_0} a^2 r} [\eta(r, t) u(r, t)]_r \quad (2.19)$$

or, in a more general form:

$$\begin{aligned} q_t(\rho, t) = & -\frac{q^2(\rho, t)}{\mu_0 \rho} \left[\frac{\eta_{\parallel}(\rho, t) \rho}{C_3^2(\rho)} \left[\frac{C_2(\rho) C_3(\rho)}{q(\rho, t)} \right]_{\rho} \right]_{\rho} \\ & + \frac{q^2(\rho, t)}{\rho} \left[\frac{\eta_{\parallel}(\rho, t) \frac{\partial \mathcal{V}}{\partial \rho}}{F C_3(\rho)} j_{ni}(\rho, t) \right]_{\rho} \end{aligned}$$

which can be obtained from (2.1) and the relation:

$$q(\rho, t) = -\frac{B_{\phi_0} \rho}{\psi_{\rho}(\rho, t)}$$

Equation (2.19) is nonlinear in q (making it difficult to extend results obtained around one equilibrium to other equilibria). This can be solved by working instead with the so-called rotational transform (denoted ι in [6], which is the inverse of the safety factor). Nevertheless, the boundary condition in the z variable (i.e. the total plasma current) can be directly (and precisely) measured using either a continuous Rogowski coil or several discrete magnetic coils around the plasma (see [6]). Therefore, in this book, we have chosen to control the safety factor profile by controlling the z variable.

2.3.3 Control Challenges

Controlling the safety factor profile q in a tokamak is done by controlling the poloidal magnetic flux profile ψ . In particular, the desired properties of the controller are:

- to guarantee the exponential stability, in a given topology, of the solutions of equation (2.15) to zero (or “close enough”) by closing the loop with a controlled input $u(\cdot, t)$;
- to be able to adjust (in particular, to accelerate) the rate of convergence of the system using the controlled input;
- to be able to determine the impact of a large class of errors motivated by the physical system and to propose a robust feedback design strategy. Actuation errors,

estimation/measurement errors, state disturbances and boundary condition errors should be considered specifically.

The problem under consideration poses several challenges that have to be addressed, some of which are:

- different orders of magnitude of the transport coefficients depending on the radial position that are also time-varying;
- strong nonlinear shape constraints imposed on the actuators and saturations on the available parameters;
- robustness of any proposed control scheme with respect to numerical problems (in particular given the difference in magnitude of the transport coefficients) and disturbances;
- coupling between the control applied to the infinite-dimensional system and the boundary condition;
- the control algorithms must be implementable in real-time (restrictions on the computational cost).

References

1. E. Witrant, E. Joffrin, S. Brémond, G. Giruzzi, D. Mazon, O. Barana, P. Moreau, A control-oriented model of the current control profile in tokamak plasma. *Plasma Phys. Control Fusion* **49**, 1075–1105 (2007)
2. F.L. Hinton, R.D. Hazeltine, Theory of plasma transport in toroidal confinement systems. *Rev. Mod. Phys.* **48**(2), 239–308 (April 1976)
3. J. Blum, *Numerical Simulation and Optimal Control in Plasma Physics*. Wiley/Gauthier-Villars *Series in Modern Applied Mathematics*. (Gauthier-Villars, Wiley, New York, 1989)
4. J.F. Artaud et al., The CRONOS suite of codes for integrated tokamak modelling. *Nucl. Fusion* **50**, 043001 (2010)
5. S.P. Hirshman, R.J. Hawryluk, B. Birge, Neoclassical conductivity of a tokamak plasma. *Nucl. Fusion* **17**(3), 611–614 (1977)
6. J. Wesson. *Tokamaks. International Series of Monographs on Physics, 118*, 3rd edn. (Oxford University Press, USA, 2004)
7. M. Erba, A. Cherubini, V.V. Parail, E. Springmann, A. Taroni, Development of a non-local model for tokamak heat transport in L-mode, H-mode and transient regimes. *Plasma Phys. Controlled Fusion* **39**(2), 261 (1997)
8. E. Witrant, S. Brémond, Shape identification for distributed parameter systems and temperature profiles in tokamaks. in *Decision and Control and European Control Conference (CDC-ECC), 2011 50th IEEE Conference* pp. 2626–2631, 2011
9. L. Laborde et al., A model-based technique for integrated real-time profile control in the JET tokamak. *Plasma Phys. Control Fusion* **47**, 155–183 (2005)
10. D. Moreau, M.L. Walker, J.R. Ferron, F. Liu, E. Schuster, J.E. Barton, M.D. Boyer, K.H. Burrell, S.M. Flanagan, P. Gohil, R.J. Groebner, C. T. Holcomb, D.A. Humphreys, A.W. Hyatt, R.D. Johnson, R.J. La Haye, J. Lohr, T.C. Luce, J.M. Park, B.G. Penaflor, W. Shi, F. Turco, W. Wehner, and ITPA-IOS group members and experts, Integrated magnetic and kinetic control of advanced tokamak plasmas on DIII-D based on data-driven models. *Nucl. Fusion* **53**:063020, 2013
11. F. Kazarian-Vibert et al., Full steady-state operation in Tore Supra. *Plasma Phys. Control Fusion* **38**, 2113–2131 (1996)

12. P. Hertout, C. Boulbe, E. Nardon, J. Blum, S. Brémond, J. Bucalossi, B. Faugeras, V. Grandgirard, P. Moreau, The CEDRES++ equilibrium code and its application to ITER, JT-60SA and Tore Supra. *Fusion Eng. Des.* **86**(6–8), 1045–1048 (2011)
13. N.J. Fisch, Theory of current drive in plasmas. *Rev. Mod. Phys.* **59**(1), 175–234 (January 1987)
14. F. Imbeaux, Etude de la propagation et de l'absorption de l'onde hybride dans un plasma de tokamak par tomographie X haute énergie. Ph.D. thesis, Université Paris XI, Orsay, France, 1999
15. O. Barana, D. Mazon, G. Caulier, D. Garnier, M. Jouve, L. Laborde, Y. Peyson, Real-time determination of suprathermal electron local emission profile from hard x-ray measurements on Tore Supra. *IEEE Trans. Nucl. Sci.* **53**, 1051–1055 (2006)
16. M. Goniche et al., Lower hybrid current drive efficiency on Tore Supra and JET. 16th Topical Conference on Radio Frequency Power in Plasmas. Park City, USA, 2005
17. S.P. Hirshman, Finite-aspect-ratio effects on the bootstrap current in tokamaks. *Phys. Fluids* **31**, 3150–3152 (1998)
18. A. Gahlawat, E. Witrant, M.M. Peet, M. Alamir, Bootstrap current optimization in tokamaks using sum-of-squares polynomials, *Proceedings of the 51st IEEE Conference on Decision and Control* (Maui, Hawaii, 2012), pp. 4359–4365
19. F. Bribiesca Argomedo, C. Prieur, E. Witrant, S. Brémond, A strict control Lyapunov function for a diffusion equation with time-varying distributed coefficients. *IEEE Trans. Autom. Control* **58**(2), 290–303 (2013)
20. A. Lunardi, *Analytic Semigroups and Optimal Regularity in Parabolic Problems, volume 16 of Progress in nonlinear differential equations and their applications.* (Birkhäuser, Basel, 1995)

Safety Factor Profile Control in a Tokamak

Bribiesca Argomedo, F.; Witrant, E.; Prieur, C.

2014, XI, 96 p. 29 illus., 24 illus. in color., Softcover

ISBN: 978-3-319-01957-4